Energy Storage Materials 16 (2019) 259–266

Contents lists available at ScienceDirect

Energy Storage Materials

journal homepage: www.elsevier.com/locate/ensm

Spatially uniform deposition of lithium metal in 3D Janus hosts

Bo Hong[a,1], Hailin Fan[b,1], Xin-Bing Cheng[c,1], Xiaolin Yan[a], Shu Hong[a], Qingyuan Dong[b], Chunhui Gao[b], Zhian Zhang[b], Yanqing Lai[b,*], Qiang Zhang[c,*]

[a] School of Materials Science and Engineering, Central South University, Changsha, Hunan 410083, China
[b] School of Metallurgy and Environment, Central South University, Changsha, Hunan 410083, China
[c] Beijing Key Laboratory of Green Chemical Reaction Engineering and Technology, Department of Chemical Engineering, Tsinghua University, Beijing 100084, China

ARTICLE INFO

Keywords:
lithium metal anodes
lithiophilic gold nanoparticles
3D carbon fiber paper
Li metal nucleation
Janus nanostructured current collectors

ABSTRACT

Three-dimensional (3D), high-specific-surface-area, and porous current collectors are strongly considered as the hosts of lithium deposition to avoid dendrite growth of lithium metal in rechargeable batteries. However, a major hurdle in these hosts is the poor affinity of lithium in non-polar framework and favorable lithium deposition toward the conductive separator-facing surface while leaving the interior voids empty. Herein, we demonstrate an effective strategy to address the issue of spatially heterogeneous lithium deposition in 3D Janus current collectors by modifying its separator-away surface with low Li/Li^+ over-potential nanoparticles as nucleation sites to guide lithium deposition. The metallic lithium preferentially nucleates around the gold nanoparticles that are sputtered on the separator-away surface of the carbon paper. The lithium metal then grows along the adjacent carbon fiber and renders it spatially homogeneous for deposition/dissolution during the repeated charge/discharge processes. The Janus gold nanoparticle-modified carbon paper (Au/CP) electrode exhibits an excellent Coulombic efficiency of 99.1% over 100 cycles at 1.0 mA cm^{-2} in the ether electrolyte, while the pristine carbon paper (CP) and stainless steel foil (SS) electrodes exhibit Coulombic efficiencies of less than 80.0% after 74 and 59 cycles, respectively. The strategy is universal and similar results are obtained when replacing gold, carbon paper, and ether electrolyte with zinc oxide, nickel foam, and carbonate electrolyte, respectively. Therefore, this strategy presents a general approach to regulate lithium ion distribution, nucleation, and deposition behavior for long-lifespan lithium metal batteries.

1. Introduction

Lithium metal is regarded as the 'holy grail' anode in high energy secondary batteries because of its high theoretical capacity (3860 mAh g^{-1}), low density (0.53 g cm^{-3}), and very negative potential (−3.04 V vs. the standard hydrogen electrode) [1–3]. Unfortunately, lithium dendrite growth, low Coulombic efficiency, and security issues limit the practical applications of lithium metal anodes into rechargeable batteries [4,5]. Various approaches including optimized electrolytes [6–11], solid state electrolyte [12–14], protected separators [15–17], surface-modified lithium foils [18,19], lithium powders [20,21], and new current collectors [22–24] have been employed to suppress the lithium dendrites and improve Coulombic efficiency of Li metal anodes.

The advanced three-dimensional (3D) porous current collectors can significantly reduce the effective current density. Consequently, the Sand's time is extended and lithium dendrite growth is suppressed. Based on this consideration, graphene [25–27], artificial graphite [28], carbon fibers [29,30], porous copper [31–34], and nickel foam [35–38] with high specific surface areas are widely considered as the hosts for lithium deposition. However, a major hurdle of these host materials is the poor affinity for lithium. Briefly, with the increase in current density and deposition capacity, the polarization of lithium metal anodes becomes strong.

To reduce the nucleation and deposition polarization, various materials are considered to enhance the affinity of these matrices with lithium metal. Cui and co-workers [39] described that gold, silver, zinc, and magnesium exhibited good metallic lithium affinity resulting in the favorable nucleation of lithium at these sites. The lithium metal preferentially nucleated and grew up on the inner gold nanoparticles rather than the outer surface of the carbon spheres. As a consequence, a high Coulombic efficiency of 98% for over 300 cycles at 0.5 mA cm^{-2} was achieved. Additionally, other lithiophilic functional groups and nanoparticles have also exhibited controllable deposition of lithium to enhance stable cycling performances. For instance, nitrogen-doped

* Corresponding authors.
E-mail addresses: laiyanqing@csu.edu.cn (Y. Lai), zhang-qiang@mails.tsinghua.edu.cn (Q. Zhang).
[1] B.H., H.L.F, and X.-B.C. contributed equally to this work.

https://doi.org/10.1016/j.ensm.2018.04.032
Received 21 March 2018; Received in revised form 15 April 2018; Accepted 29 April 2018
Available online 01 May 2018

graphene [40], ZnO quantum dots [41], and Ag nanoseeds [42] were introduced into the lithium metal anodes for highly stable lithium metal batteries.

These 3D host materials with lithiophilic functional groups or nanoparticles have uniformly dispersed nucleation sites. However, the preferential lithium nucleation and growth occur on the nanostructured Li metals at the conductive separator-facing surface (SF surface) [29,43–45]. This reduces the utilization of interior voids and leads to performance degradation. Insulating layers (SiC and Al_2O_3) [29,46] on the SF surface of the 3D hosts can prevent lithium nucleation on these surfaces and accommodate lithium deposition inside the voids. However, this strategy sacrifices the part of the surface area on the insulating layer of the coated electrode and induces strong polarization. Therefore, an efficient matrix is urgently requested to realize the uniform deposition of lithium metal in the entire spaces of 3D hosts.

In this contribution, we demonstrate a Janus 3D current collector with one lithiophilic surface and another lithiophobic surface is proposed to guide spatially heterogeneous lithium deposition. In general, such Janus current collectors can be achieved by sputtering lithiophilic nanoparticles (e.g. gold or zinc oxide) on its separator-away (SA) surface as nucleation sites to guide uniform lithium deposition. The sputtered nanoparticles have a low nucleation over-potential. Therefore, lithium ions tend to deposit on the SA surface of 3D host, rather than its SF surface. Consequently, this renders a uniform deposition of lithium ions in entire 3D hosts. Relative to the 3D hosts with tunable lithiophilic/lithiophobic chemistry [39–42] or insulating surface [29,46], the proposed strategy can not only successfully deposit lithium on the SA surface, but also reduce the polarization with the entire host utilized. The concept is proofed by Au/CP host for spatially homogeneous 3D lithium metal anode. Metallic lithium preferentially nucleates on the sputtered gold nanoparticles at the SA surface of the carbon paper electrode. The fresh lithium is then continuously deposited on these nucleation sites and grows along the adjacent carbon fibers from the SA to SF surface. Overall, this renders spatially homogeneous deposition/dissolution during the repeated charge/discharge processes (Fig. 1(a)). On the contrary, the untreated CP electrode tends to deposit lithium metal on the SF surface where lithium ions accept electrons rapidly [29,43–45]. This leads to low utilization of the interior voids and even vast growth of lithium dendrites during the repeated charge/discharge processes (Fig. 1(b)).

2. Experimental

2.1. Preparation of 3D Janus host with one lithiophilic surface and another lithiophobic surface

Au modified carbon paper (Au/CP) was prepared by sputtering Au nanoparticles on one side of carbon paper (CeTech Co., Ltd.) with an ion sputtering instrument (JFC-1600, Auto Fine Coater) at 20 mA for 200 s. Before modification, the carbon paper was ultrasonically cleaned in alcohol. As a control, stainless steel (SS) and pristine CP were treated similarly. Similar to the preparation of Au/CP, the gold-modified nickel foam (Au/Ni foam) was prepared by sputtering gold nanoparticles on one side of the commercialized nickel foam (Taiyuan Liyuan Lithium Technology Center Co., Ltd.) under identical conditions, and the Au contents on these hosts are about 0.014 mg cm^{-2}. As for zinc oxide-modified carbon paper (ZnO/CP), zinc oxide nanoparticles were deposited on one side of the commercialized carbon paper with a magnetron sputtering system under an argon atmosphere at ~1.0 Pa with a sputtering power of 80 W for 15 s with the zinc oxide target (50.8 mm in diameter and 5.0 mm in thickness) as the zinc oxide source. The mass loading of ZnO nanoparticles is about 0.031 mg cm^{-2}.

2.2. Characterization

The microscopic morphology and structure of the electrodes were characterized by scanning electron microscopy (SEM, FEI Nova NanoSEM 230) and energy dispersive spectrometer (EDS). The 2025-type coin cells were composed of SS, CP, Au/CP, and ZnO/CP as the working electrode, lithium foil as the counter/reference electrode, a Celgard 2400 separator, and electrolyte of 1.0 M lithium bis(trifluoromethane-sulfonyl)imide (LiTFSI) in 1,2-dimethoxyethane (DME)/ 1,3-dioxolane (DOL) (1:1 by volume) with 1.0 wt.% $LiNO_3$ as typical in a lithium–sulfur battery. To prevent the penetration of the Celgard 2400 separator, working electrodes of Ni foam and Au/Ni foam were assembled in 2032-type cell coins with a glass fiber separator. 60 µl electrolyte was used in 2025-type coin cells and 150 µl electrolyte was used in 2032-type coin cells. For convenience of comparison, we defined the host surface placed away from separator as the SA surface, and the surface near the separator as the SF surface. For Au/CP, Au/Ni foam, and ZnO/CP hosts, the surfaces with gold or zinc oxide nanoparticle modification were the SA surfaces. Galvanostatic cycling performance was measured by a LAND CT2001A battery-testing

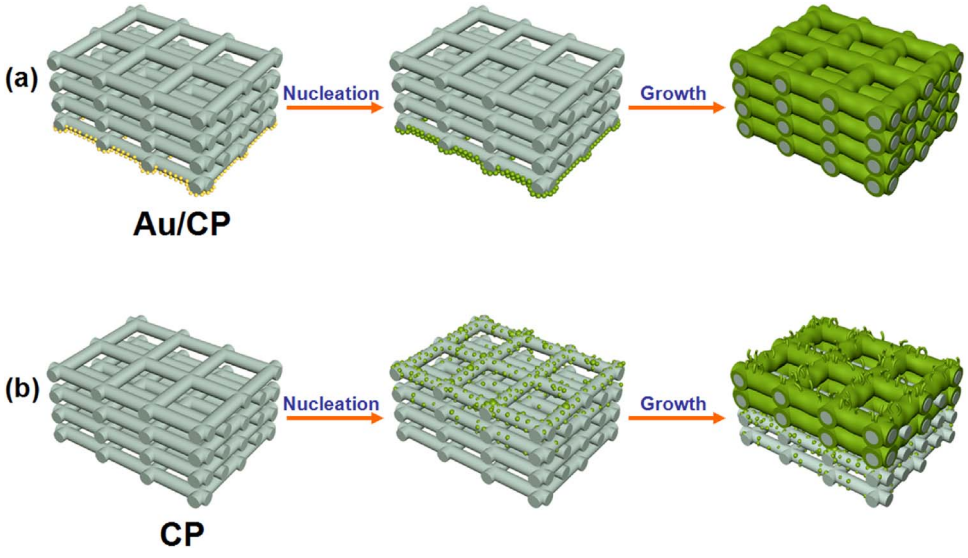

Fig. 1. Schematic diagram of lithium nucleation and growth in the Au/CP (a) and CP (b) host.

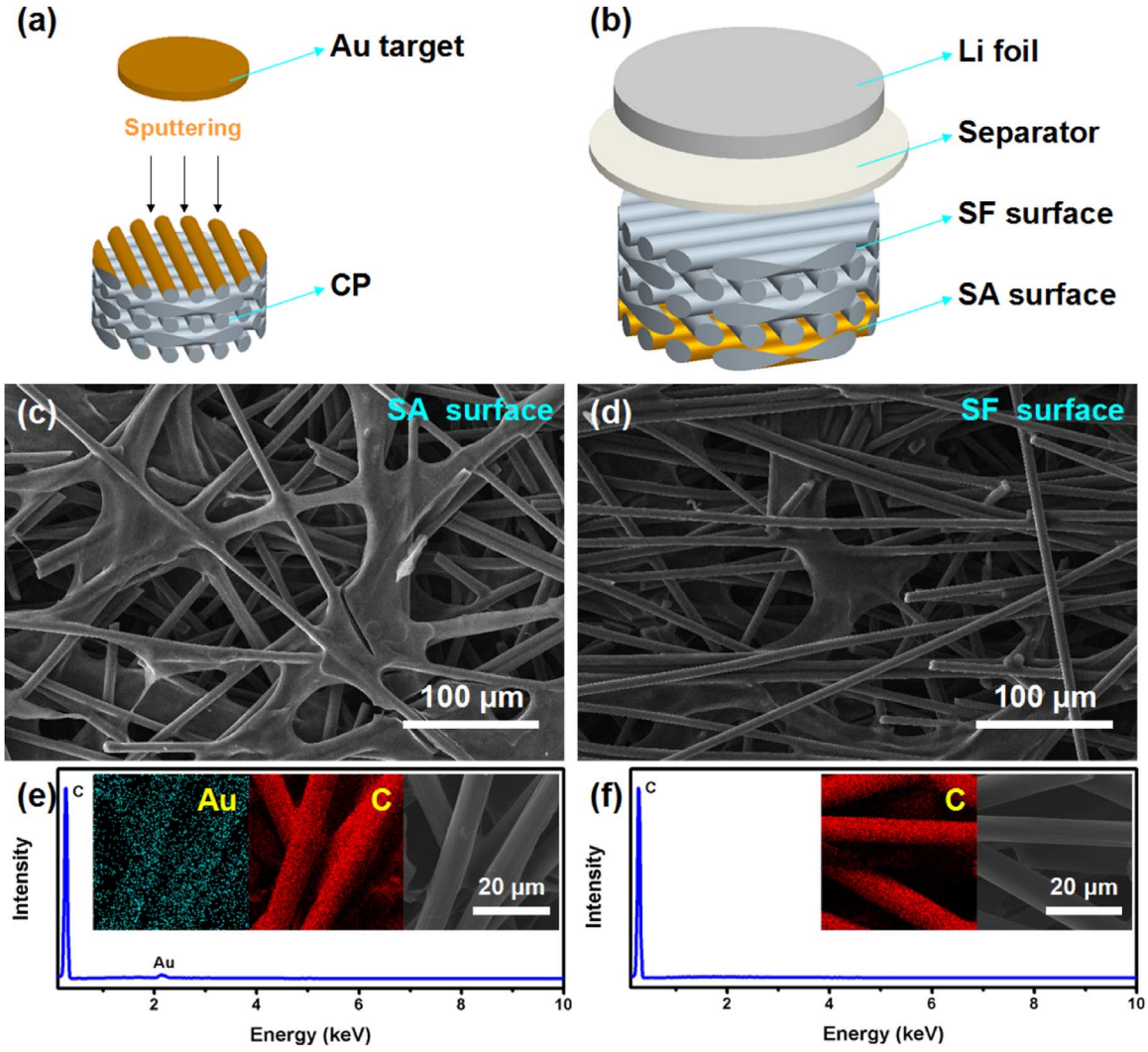

Fig. 2. Schematic diagram of gold sputtering on the CP (a) and the Li metal battery using Au/CP electrode (b). SEM images of Au/CP on the SA surface (c) and SF surface (d). EDS spectrograms of Au/CP on the SA surface (e) and SF surface (f).

instrument at room temperature (25 °C). The lithiation capacity was 1.0 and 3.0 mAh cm^{-2} at 0.2, 0.5, 1.0, 2.0, 3.0, and 5.0 mA cm^{-2}, and the delithiation potential was 1.0 V at the same current. The Coulombic efficiency was calculated as the ratio of the delithiation capacity versus the lithiation capacity. The full Li metal battery herein is with $LiFePO_4$ (Taiyuan Liyuan Lithium Technology Center Co., Ltd.) and composite Li metal anode. The $LiFePO_4$, PVDF binder and carbon black in a weight ratio of 8:1:1 were dissolved into N-methyl-2-pyrrolione to obtain the electrode with a mass loading of $LiFePO_4$ of ~8.0 mg cm^{-2}. Electrochemical impedance spectroscopy (EIS) measurements were conducted by Solartron 1470E cell test system from 100 kHz to 10 mHz.

3. Results and discussion

3.1. Morphology and structure of Au/CP host

Au/CP host is prepared by sputtering Au nanoparticles on one side of the CP (Fig. 2(a)). The surface with Au modification is placed away from separator as the SA surface (Fig. 2(b)). SEM images of Au/CP hosts for the SA and SF surfaces are shown in Fig. 2(c) and (d), respectively. The CP are consisted of ca. 7 μm carbon fibers with an open porous structure. After Au sputtering, the Au nanoparticles are evenly distributed on the SA surface of the carbon paper, and no Au is found on the SF surface (see Fig. 2(e), (f) and their insets). Additionally, the loading of Au nanoparticles is only about 0.014 mg cm^{-2} by weight in the Au/CP host after 10 rounds of Au sputtering, rendering no change of CP electrode (Fig. S1(a) and (b)). These Au nanoparticles are expected to induce preferential nucleation and growth of lithium metal [39,47].

3.2. Lithium depositing morphology

To investigate the deposition behavior of lithium metal on the CP and Au/CP electrodes, a continuous deposition test is performed at 0.1 mA cm^{-2} with different capacities (0.1, 0.5, and 1.0 mAh cm^{-2}). Fig. S2 exhibits the "geographical" distribution of the deposited lithium metal on the CP electrodes after different deposition durations. Metallic lithium progressively appears on the SF surface when plating 0.1 mAh cm^{-2} lithium at the CP electrode (Fig. S2(a)). However, there is few morphology changes on the SA surface (Fig. S2(d) and (g)). As the deposition capacity increases to 0.5 and 1.0 mAh cm^{-2}, the lithium particles gradually grow into large lumps and are distributed in the voids close to the SF surface (Fig. S2(b) and (c)), resulting in an obviously increased thickness of the carbon fibers; only a trace of metallic lithium is deposited on the SA surface (Fig. S2(e), (f), (h), and (i)). This indicates that the metallic lithium preferentially deposits and grows on the SF surface of the CP electrode because of the short pathways for lithium ions to accept the electrons [29]. This uneven deposition of the lithium reduces the utilization of the interior voids

and induces performance degradation of the CP electrode during the repeated charge/discharge cycling.

In a sharp contrast, lithium deposition behavior on the Janus Au/CP electrode is completely different (Fig. S3). The metallic lithium is preferentially deposited (Fig. S3(d)) on the SA surface, but not on the SF surface at a low deposition capacity of 0.1 mAh cm^{-2} (Fig. S3(a) and (g)). This means gold nanoparticles regulate the favorable deposition sites by inducing nucleation of metallic lithium because of its low lithium deposition over-potential [39]. When the deposition capacity increases to 0.5 mAh cm^{-2}, the metallic lithium coverage area gradually increases (Fig. S3(h)). Meanwhile, more metallic lithium is deposited on the carbon fibers of the SA surface (Fig. S3(e)). However, carbon fibers on the SF surface are still smooth indicating that no metallic lithium is deposited (Fig. S3(b)). When the deposition capacity increases to 1.0 mAh cm^{-2}, the metallic lithium is evenly covered on all carbon fibers either on the SA surface or on the SF surface (Fig. S3(c), (f), and (i)). Besides, the Au/CP electrode exhibits a small thickness change compared to the thickness of CP electrode after lithium deposition. This indicates that lithium is mainly deposited inside the spacious voids.

When the deposition capacity increases to 3.0 mAh cm^{-2} at a high current density of 3.0 mA cm^{-2}, the contrasts between CP and Au/CP electrode are more obvious. Negligible metallic lithium is deposited on the SA surface for CP electrode (Fig. 3(a), (b), and Fig. S4(a)), indicating lithium deposition mainly on the SF surface. On the contrary, metallic lithium is uniformly deposited on the SA surface as well as SF surface of Au/CP electrode (Fig. 3(d), (e), and Fig. S4(b)). Furthermore, the Au/CP electrode displays smaller thickness (137.1 μm) (Fig. 3(f)) than CP electrode (142.9 μm) (Fig. 3(c)) after lithium deposition. This is ascribed to the fact that lithium can homogeneously deposit into the interior of Au/CP host, rather than only the surface of CP host. All these results confirm that metallic lithium is preferentially nucleated on the Au nanoparticles, and then grow evenly along the carbon fibers from the SA surface to the SF surface.

3.3. Long-term electrochemical performance

To confirm the concept of the uniform lithium deposition into Janus 3D current collector with one lithiophilic surface and another lithiophobic surface during long term cycling, the cycling performances of CP and Au/CP electrodes are recorded under different current densities (0.2, 0.5, 1.0, and 2.0 mA cm^{-2}) (Fig. 4). The SS electrode is also selected as the control sample. The SS electrode exhibits low average Coulombic efficiencies of 92.6% and 87.4% at 0.2 and 0.5 mA cm^{-2} (Fig. 4(a) and (b)), respectively, after 100 cycles. When the current density increases to 1.0 mA cm^{-2}, the SS electrode shows a Coulombic efficiency of less than 80.0% after 59 cycles (Fig. 4(c)). Even worse, the battery quickly fails when the current density increases to 2.0 mA cm^{-2} (Fig. 4(d)).

In contrast, the CP electrode shows a high Coulombic efficiency of 98.9% at 0.2 mA cm^{-2} after 100 cycles (Fig. 4(a)). This significantly outperforms the SS electrode for the reason that CP exhibits high surface area, large void volume, and good electrical conductivity, which will reduce the effective current density and enhance electrolyte uptake capabilities [27,48,49]. Besides, polar surface functional groups (such as C-O and C=O) are still found on the CP electrode (Fig. S5), which may attract lithium ion and form additional electrical fields to relieve the tip effect as well as facilitate well-distributed homogeneous lithium ionic flux during the lithium deposition [50–53]. All these reasons are benefited for uniform lithium metal deposition. Unfortunately, when

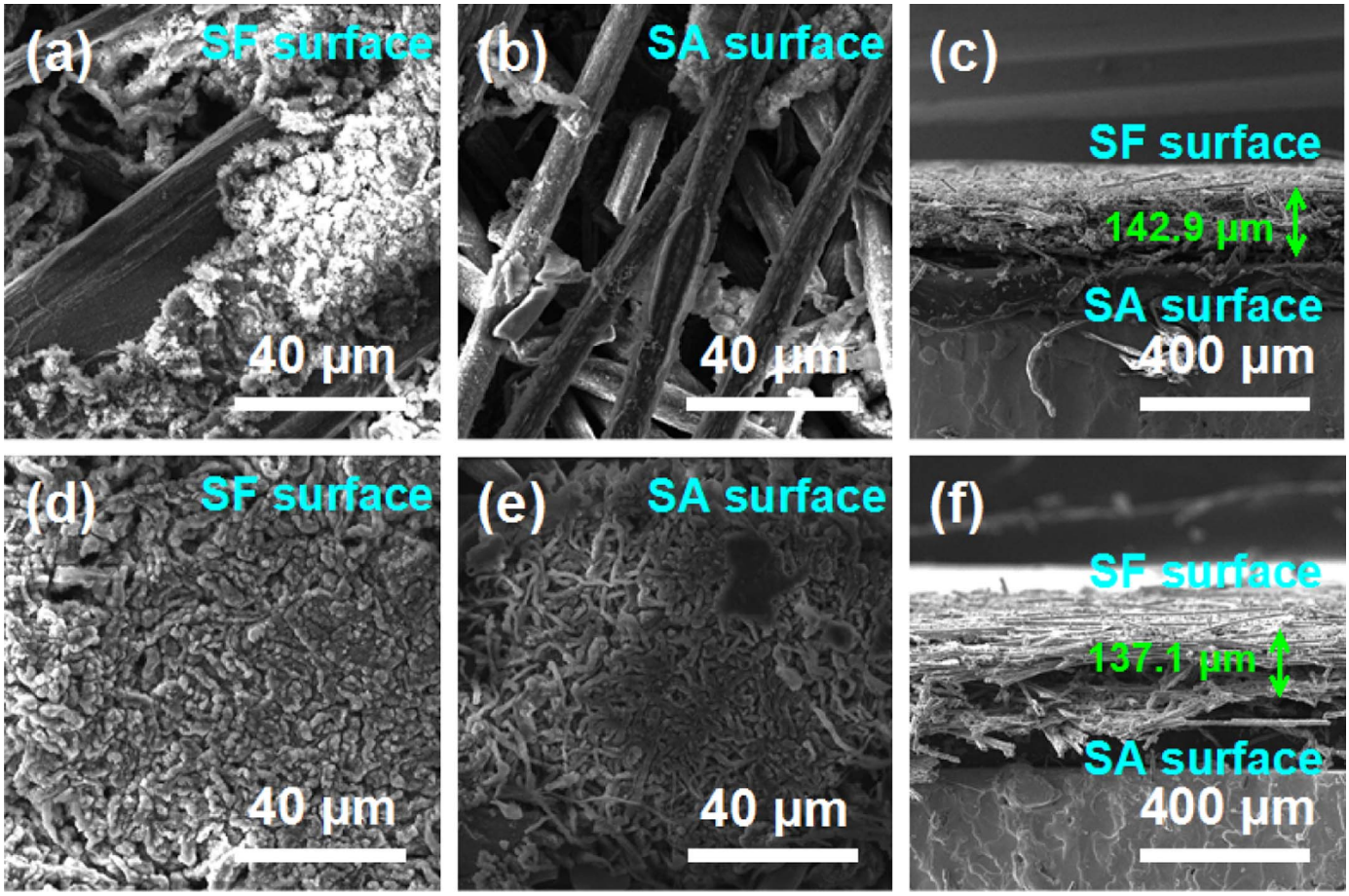

Fig. 3. SEM images of CP (a-c) and Au/CP (d-f) electrodes on the SF/SA surfaces and at the cross section with 3.0 mAh cm^{-2} deposited at 3.0 mA cm^{-2}.

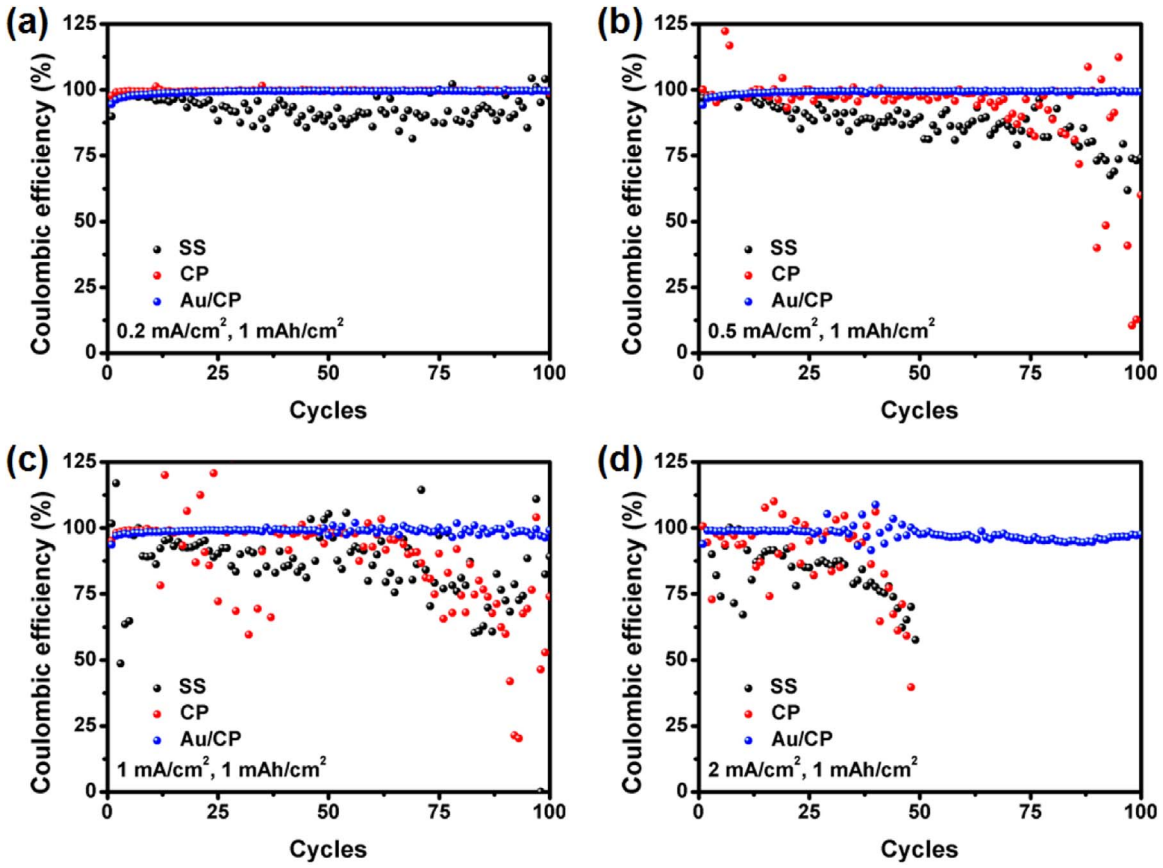

Fig. 4. Electrochemical performances of SS, CP, and Au/CP electrodes at 0.2 (a), 0.5 (b), 1.0 (c), and 2.0 mA cm^{-2} (d).

the current density increases to 0.5 and 1.0 mA cm^{-2}, the lithium metal are non-uniformly deposited on the CP electrode. While the CP electrode exhibits average Coulombic efficiencies of 93.0% and 89.0% at 0.5 and 1.0 mA cm^{-2}, respectively, the Coulombic efficiencies quickly drops to less than 80.0% after 86 and 74 cycles, respectively (Fig. 4(b) and (c)). With further increase of current density (2.0 mA cm^{-2}), the CP electrode quickly fails, shown in Fig. 4(d).

Specifically, once Janus Au/CP electrode is applied, the cells exhibit high Coulombic efficiencies of 99.5%, 99.3%, 99.1%, and 97.6% at 0.2, 0.5, 1.0, and 2.0 mA cm^{-2}, after 100 cycles (Fig. 4(a), (b), (c) and (d)), respectively. This is much higher than that on the SS and CP electrodes. Furthermore, the Janus Au/CP electrode still has high average Coulombic efficiency of 97.2% after 100 cycles even at a high current density (3.0 mA cm^{-2}) and high area capacities (3.0 mAh cm^{-2}), whereas the CP electrode exhibits a Coulombic efficiency of less than 80.0% only after 35 cycles (Fig. S6). Besides, the Au/CP electrode shows minimum charge transfer resistance before and after 40 cycles (Fig. S7). These results indicate that Au nanoparticles induces uniform lithium nucleation and growth in the interior voids to improve the spatial homogeneity and utilization of interior voids and further enhance the performance of the CP electrode.

In order to understand the failure mechanism of these batteries as well as to confirm the inducing effect of gold nanoparticles on carbon paper, SEM images of SS, CP, and Au/CP electrodes on the surface and at a cross section after 40 cycles with a current density of 1.0 mA cm^{-2} are shown in Fig. 5. There are residual impurities on the SS surface or among the carbon fibers, which are corresponding to mossy lithium that consists of electrolyte reduction products and dead lithium. The SS electrode has inherent shortcomings of 2D current collectors and is prone to induce unstable lithium particle nucleation and growth. This is followed by the growth of lithium dendrites during repeated charge/discharge cycles [54,55]. As a result, abundant cracks, dead lithium and mossy lithium layers with a thickness of about 27.3 μm are found on the SF surface (Fig. 5(a) and (b)). More promisingly, these accumulated dead lithium and mossy lithium reduce the Coulombic efficiency of the SS electrode.

As for CP electrode, the porous structure on the SF surface is almost completely filled by mossy lithium and dead lithium (Fig. 5(c)), resulting in increased thickness of CP electrode from about 133.5 (Fig. S1(b)) to 144.3 μm (Fig. 5(d)) after 40 cycles. Both dead lithium and mossy lithium are mainly distributed in the SF region of this electrode (cross section (Fig. 5(d)). This strongly proves that the carbon fiber located in the SF region offers favorable sites for lithium deposition and dendrite growth. Unlike the CP electrode, the thickness of the Janus Au/CP electrode is only 133.7 μm, rendering almost no expansion after 40 cycles. Also, there is little dead lithium or mossy lithium on the Janus Au/CP electrode surface or among the carbon fibers (Fig. 5(e) and (f)), which is consistent with its high Coulombic efficiency exhibited in Fig. 4(c).

We also tests the Coulombic efficiencies of SS, CP, and Au/CP electrodes in an alkyl carbonate electrolyte that is usually used for lithium ion batteries (Fig. S8**)**. An average Coulombic efficiency of 94.7% over 120 cycles is obtained at 1.0 mA cm^{-2} with a lithium capacity of 1.0 mAh cm^{-2} on the Janus Au/CP electrode. In contrast, the Coulombic efficiency decreases to less than 80.0% after 40 cycles for the SS electrode and 94 cycles for the CP electrode. Similarly, when $LiFePO_4$ is adopted as the lithium source, the Au/CP electrode renders a high and stable Coulombic efficiency of 99.6% with a discharge capacity of 45.3 mAh g^{-1} at 0.5 C after 500 cycles, whereas the CP electrode displays an unstable Coulombic efficiency and low discharge capacity of < 40.0 mAh g^{-1} only after 20 cycles (Fig. S9). Therefore, Au nanoparticle-modified carbon paper offers potential applications in the practical lithium metal batteries without Li dendrite formation.

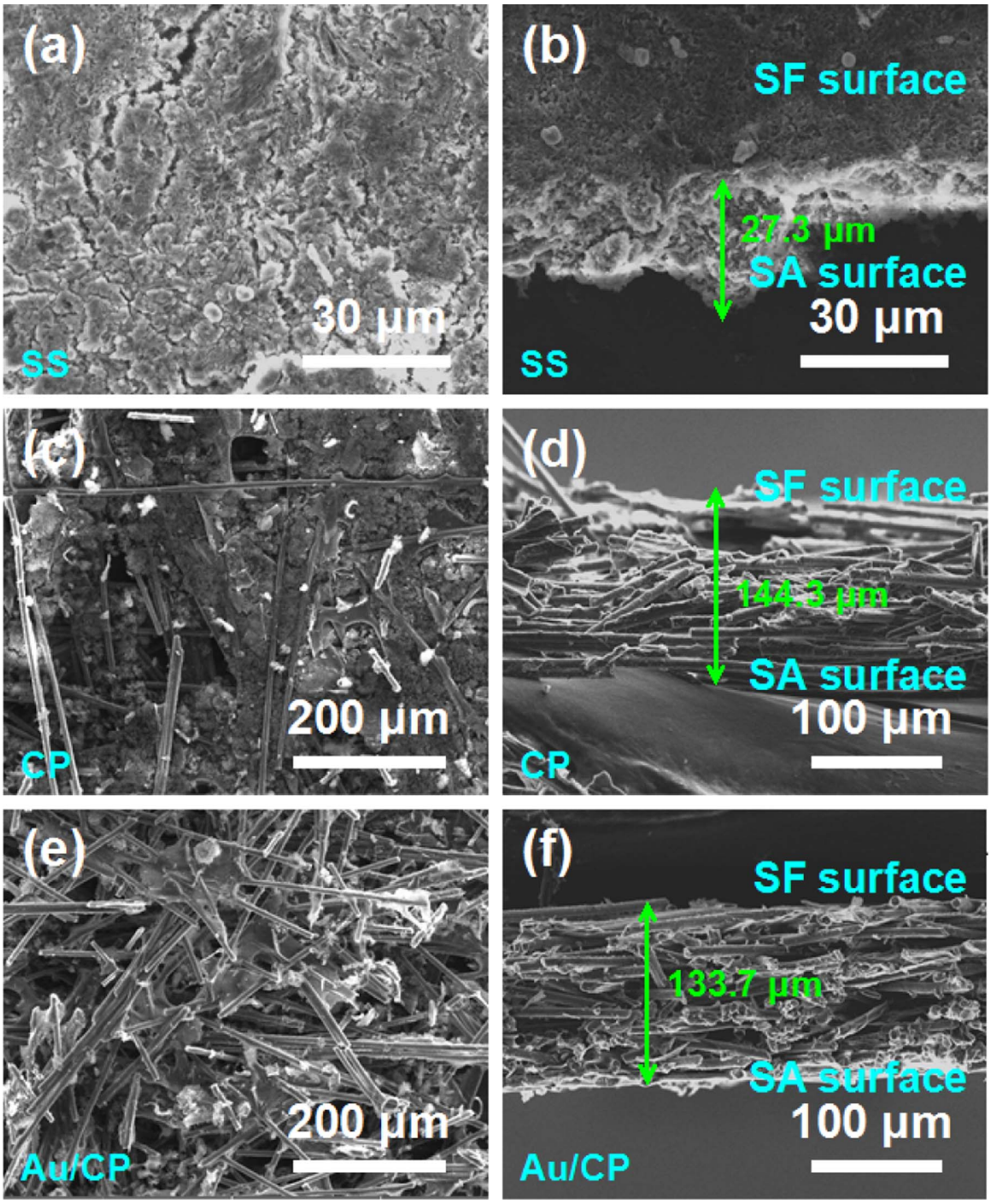

Fig. 5. SEM images of SS electrode on the SF surface (a) and at the cross section (b), CP electrode on the SF surface (c) and at the cross section (d), Au/CP electrode on the SF surface (e) and at the cross section (f) after 40 cycles at 1.0 mA cm^{-2} and 1.0 mAh cm^{-2}.

3.4. Strategy prolongation

To illustrate the general Janus current collector strategy, we employ nickel foam modified with gold nanoparticles as a 3D current collector (Fig. 6(a-d)). A high Coulombic efficiency of 99.4% for nearly 250 cycles at 2.0 mA cm^{-2} in an ether electrolyte is achieved on the Janus Au/Ni foam current collectors (Fig. 6(e). Even if the current density is increased to the practical current density of commercial lithium metal batteries (5.0 mA cm^{-2}), the Au/Ni foam electrode still shows an average Coulombic efficiency of 96.6% for nearly 180 cycles (Fig. 6(f)). In contrast, pristine nickel foam electrode without gold nanoparticle modification exhibits Coulombic efficiencies of less than 80.0% after 60 cycles at 2.0 mA cm^{-2} or 50 cycles at 5.0 mA cm^{-2}, respectively.

In addition, we further employ lithiophilic zinc oxide nanoparticle [56]-modified CP as a host material for dendrite-free lithium deposition (Fig. S10 and Fig. S11). The zinc oxide is easily reduced to zinc ($2Li^+ + ZnO + 2e \rightarrow Li_2O + Zn$) during the lithium deposition [41,57]. Consequently, the ZnO/CP electrode renders an average Coulombic efficiency of 98.6% over 100 cycles because of the preferentially induced lithium nucleation and growth on the zinc nanoparticles [40], which is far better than the performance of CP electrode. (Fig. S12). Therefore, this strategy to regulate lithium deposition is effective in a family of 3D Janus current collectors.

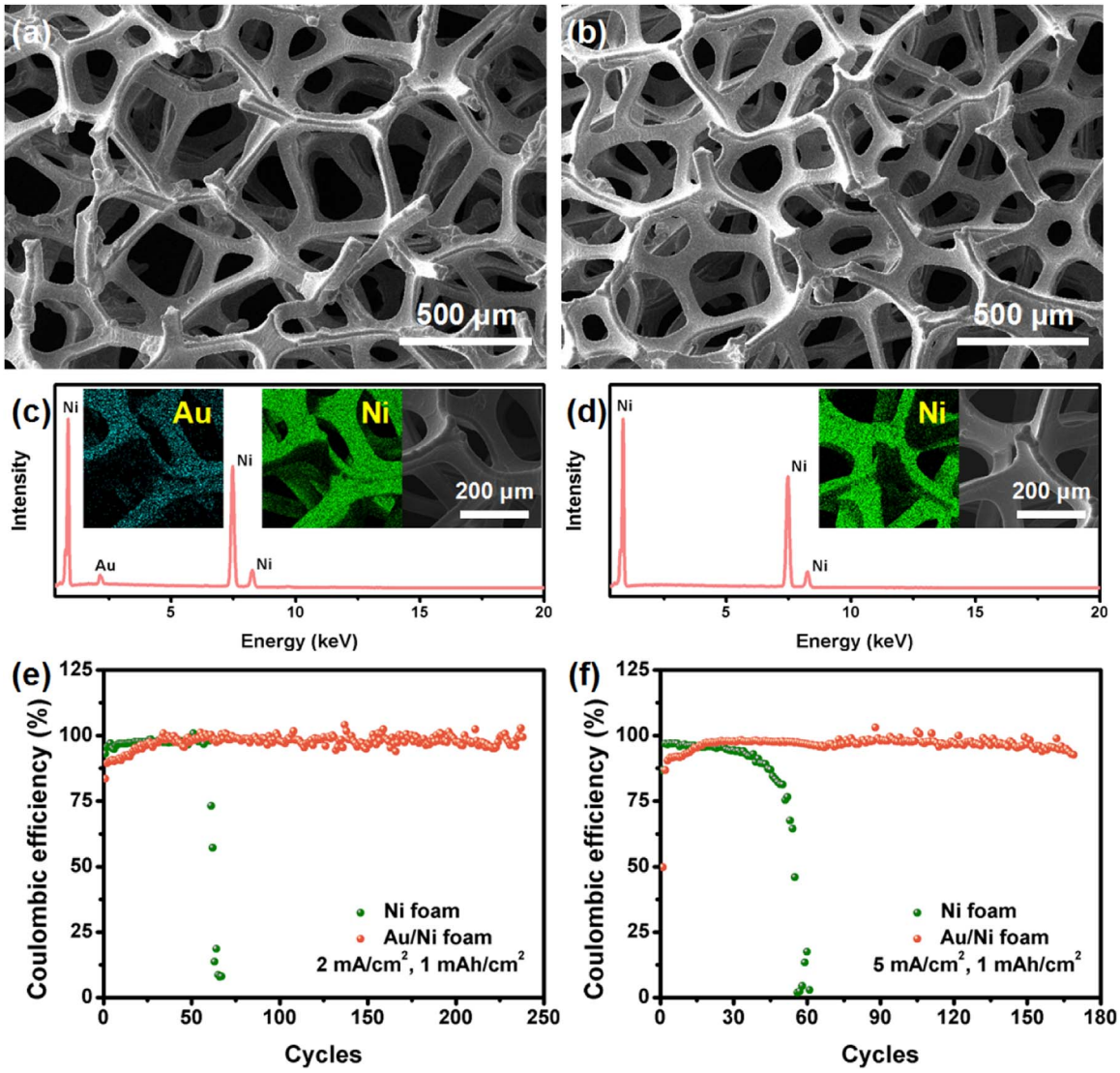

Fig. 6. SEM images of Au/Ni foam on the SA surface (a) and SF surface (b). EDS spectrograms of Au/Ni on the SA surface (c) and SF surface (d). Electrochemical performance of Ni foam and Au/Ni foam electrodes in a half-cell at 2.0 and 5.0 mA cm^{-2} (e and f).

4. Conclusion

We demonstrate a general concept to guide spatially lithium metal deposition in the interior of Janus 3D hosts with one lithiophilic surface and another lithiophobic surface. The Janus 3D CP electrode is modified by uniform Au nanoparticles via a facile Au sputtering onto its SA surface. Due to the lithiophilic feature of these Au nanoparticles, lithium ions preferentially nucleates on these Au nanoparticles. Therefore, the metallic lithium is guided to these sites for continuous and uniform deposition. Then the Li metal grows evenly along the carbon fibers from the SA surface to the SF surface and finally realizes a uniform deposition in the entire 3D Janus host rather than only on the SF surface. As a result, the Au/CP electrode shows Coulombic efficiencies of 99.5%, 99.3%, 99.1%, and 97.6% after 100 cycles at 0.2, 0.5, 1.0, and 2.0 mA cm^{-2}, respectively. These values are much higher than these of SS and 3D CP electrodes. After replacing gold with inexpensive zinc oxide and carbon paper with nickel foam, the Au/Ni foam electrode offers a lifespan of nearly 250 and 180 cycles at 2.0 and 5.0 mA cm^{-2}, respectively. Furthermore, when $LiFePO_4$ was adopted as the lithium source, the Janus Au/CP electrode exhibits a high and stable Coulombic efficiency of 99.6%, while the CP electrode displays an unstable Coulombic efficiency only after 20 cycles. Therefore, this strategy is an effective method to regulate lithium deposition in a working lithium metal anode. To summarize, it is a fundamental concept to overcome the spatially heterogeneous deposition and even dendrite growth toward the conductive SF surface while leaving the interior voids empty in 3D hosts in a working Li metal battery.

Acknowledgments

The authors thank the financial support from the National Natural Science Foundation of China (51720105014), National Key Research and Development Program (2016YFA0202500), China Postdoctoral Science Foundation (2017M620773 and BX201700125), and Fundamental Research Funds for the Central Universities of Central South University (No. 2018zzts138).

Appendix A. Supplementary material

Supplementary data associated with this article can be found in the online version at doi:10.1016/j.ensm.2018.04.032.

References

[1] A.C. Luntz, B.D. McCloskey, Chem. Rev. 114 (2014) 11721–11750.
[2] R. Cao, W. Xu, D. Lv, J. Xiao, J.-G. Zhang, Adv. Energy Mater. 5 (2015) 1402273.

[3] J.W. Choi, D. Aurbach, Nat. Rev. Mater. 1 (2016) 16013.
[4] X.-B. Cheng, R. Zhang, C.-Z. Zhao, Q. Zhang, Chem. Rev. 117 (2017) 10403–10473.
[5] X.-B. Cheng, C. Yan, J.-Q. Huang, P. Li, L. Zhu, L. Zhao, Y. Zhang, W. Zhu, S.-T. Yang, Q. Zhang, Energy Storage Mater. 6 (2017) 18–25.
[6] X.-B. Cheng, M.-Q. Zhao, C. Chen, A. Pentecost, K. Maleski, T. Mathis, X.-Q. Zhang, Q. Zhang, J. Jiang, Y. Gogotsi, Nat. Commun. 8 (2017) 336–344.
[7] C.-Z. Zhao, X.-B. Cheng, R. Zhang, H.-J. Peng, J.-Q. Huang, R. Ran, Z.-H. Huang, F. Wei, Q. Zhang, Energy Storage Mater. 3 (2016) 77–84.
[8] X.-B. Cheng, C. Yan, H.-J. Peng, J.-Q. Huang, S.-T. Yang, Q. Zhang, Energy Storage Mater. 10 (2018) 199–205.
[9] L. Suo, Y.-S. Hu, H. Li, M. Armand, L. Chen, Nat. Commun. 4 (2013) 1481–1489.
[10] C.S. Rustomji, Y. Yang, T.K. Kim, J. Mac, Y.J. Kim, E. Caldwell, H. Chung, Y.S. Meng, Science 356 (2017) 1351.
[11] F. Ding, W. Xu, G.L. Graff, J. Zhang, M.L. Sushko, X. Chen, Y. Shao, M.H. Engelhard, Z. Nie, J. Xiao, X. Liu, P.V. Sushko, J. Liu, J.-G. Zhang, J. Am. Chem. Soc. 135 (2013) 4450–4456.
[12] X.-X. Zeng, Y.-X. Yin, N.-W. Li, W.-C. Du, Y.-G. Guo, L.-J. Wan, J. Am. Chem. Soc. 138 (2016) 15825–15828.
[13] F. Shen, M.B. Dixit, X. Xiao, K.B. Hatzell, ACS Energy Lett. 3 (2018) 1056–1061.
[14] Y. Tian, F. Ding, H. Zhong, C. Liu, Y.-B. He, J. Liu, X. Liu, Q. Xu, Energy Storage Mater. 14 (2018) 49–57.
[15] W. Luo, L. Zhou, K. Fu, Z. Yang, J. Wan, M. Manno, Y. Yao, H. Zhu, B. Yang, L. Hu, Nano Lett. 15 (2015) 6149–6154.
[16] M.-H. Ryou, D.J. Lee, J.-N. Lee, Y.M. Lee, J.-K. Park, J.W. Choi, Adv. Energy Mater. 2 (2012) 645–650.
[17] P. Bai, J. Li, F.R. Brushett, M.Z. Bazant, Energ. Environ. Sci. 9 (2016) 3221–3229.
[18] N.-W. Li, Y.-X. Yin, C.-P. Yang, Y.-G. Guo, Adv. Mater. 28 (2016) 1853–1858.
[19] A.C. Kozen, C.-F. Lin, A.J. Pearse, M.A. Schroeder, X. Han, L. Hu, S.-B. Lee, G.W. Rubloff, M. Noked, ACS Nano 9 (2015) 5884–5892.
[20] C.W. Kwon, S.E. Cheon, J.M. Song, H.T. Kim, K.B. Kim, C.B. Shin, S.W. Kim, J. Power Sources 93 (2001) 145–150.
[21] J. Heine, S. Krüger, C. Hartnig, U. Wietelmann, M. Winter, P. Bieker, Adv. Energy Mater. 4 (2014) 1300815.
[22] T.-T. Zuo, X.-W. Wu, C.-P. Yang, Y.-X. Yin, H. Ye, N.-W. Li, Y.-G. Guo, Adv. Mater. 29 (2017) 1700389.
[23] X.-Q. Zhang, X. Chen, R. Xu, X.-B. Cheng, H.-J. Peng, R. Zhang, J.-Q. Huang, Q. Zhang, Angew. Chem. Int. Ed. 56 (2017) 14207–14211.
[24] Y. Zhang, W. Luo, C. Wang, Y. Li, C. Chen, J. Song, J. Dai, E.M. Hitz, S. Xu, C. Yang, Y. Wang, L. Hu, P. Nat. Acad. Sci. 114 (2017) 3584–3589.
[25] D. Lin, Y. Liu, Z. Liang, H.-W. Lee, J. Sun, H. Wang, K. Yan, J. Xie, Y. Cui, Nat. Nanotechnol. 11 (2016) 626–632.
[26] X.-B. Cheng, H.-J. Peng, J.-Q. Huang, R. Zhang, C.-Z. Zhao, Q. Zhang, ACS Nano 9 (2015) 6373–6382.
[27] R. Zhang, X.-B. Cheng, C.-Z. Zhao, H.-J. Peng, J.-L. Shi, J.-Q. Huang, J. Wang, F. Wei, Q. Zhang, Adv. Mater. 28 (2016) 2155–2162.
[28] Y. Sun, G. Zheng, Zhi W. Seh, N. Liu, S. Wang, J. Sun, Hye R. Lee, Y. Cui, Chem 1 (2016) 287–297.
[29] X. Ji, D.-Y. Liu, D.G. Prendiville, Y. Zhang, X. Liu, G.D. Stucky, Nano Today 7 (2012) 10–20.
[30] A. Zhang, X. Fang, C. Shen, Y. Liu, C. Zhou, Nano Res. 9 (2016) 3428–3436.
[31] C.-P. Yang, Y.-X. Yin, S.-F. Zhang, N.-W. Li, Y.-G. Guo, Nat. Commun. 6 (2015) 8058–8066.
[32] Q. Yun, Y.-B. He, W. Lv, Y. Zhao, B. Li, F. Kang, Q.-H. Yang, Adv. Mater. 28 (2016) 6932–6939.
[33] L.L. Lu, J. Ge, J.N. Yang, S.M. Chen, H.B. Yao, F. Zhou, S.H. Yu, Nano Lett. 16 (2016) 4431–4437.
[34] Q. Li, S. Zhu, Y. Lu, Adv. Funct. Mater. 27 (2017) 1606422.
[35] C. Wang, D. Wang, C. Dai, J. Electrochem. Soc. 155 (2008) A390–A394.
[36] K. Xie, W. Wei, K. Yuan, W. Lu, M. Guo, Z. Li, Q. Song, X.-R. Liu, J.-G. Wang, C. Shen, ACS Appl. Mater. Inter. 8 (2016) 26091–26097.
[37] S.-S. Chi, Y. Liu, W.-L. Song, L.-Z. Fan, Q. Zhang, Adv. Funct. Mater. 27 (2017) 1700348.
[38] H. Ye, S. Xin, Y.-X. Yin, J.-Y. Li, Y.-G. Guo, L.-J. Wan, J. Am. Chem. Soc. 139 (2017) 5916–5922.
[39] K. Yan, Z. Lu, H.-W. Lee, F. Xiong, P.-C. Hsu, Y. Li, J. Zhao, S. Chu, Y. Cui, Nat. Energy 1 (2016) 16010.
[40] R. Zhang, X.-R. Chen, X. Chen, X.-B. Cheng, X.-Q. Zhang, C. Yan, Q. Zhang, Angew. Chem. Int. Ed. 56 (2017) 7764–7768.
[41] C. Jin, O. Sheng, J. Luo, H. Yuan, C. Fang, W. Zhang, H. Huang, Y. Gan, Y. Xia, C. Liang, J. Zhang, X. Tao, Nano Energy 37 (2017) 177–186.
[42] C. Yang, Y. Yao, S. He, H. Xie, E. Hitz, L. Hu, Adv. Mater. 29 (2017) 1702714.
[43] Y. Liu, D. Lin, Z. Liang, J. Zhao, K. Yan, Y. Cui, Nat. Commun. 7 (2016) 10992–11000.
[44] C. Zhang, Z. Huang, W. Lv, Q. Yun, F. Kang, Q.-H. Yang, Carbon 123 (2017) 744–755.
[45] H. Lee, J. Song, Y.-J. Kim, J.-K. Park, H.-T. Kim, Sci. Rep. 6 (2016) 30830–30839.
[46] Y. Zhang, B. Liu, E. Hitz, W. Luo, Y. Yao, Y. Li, J. Dai, C. Chen, Y. Wang, C. Yang, H. Li, L. Hu, Nano Res. 10 (2017) 1356–1365.
[47] L. Porz, T. Swamy, B.W. Sheldon, D. Rettenwander, T. Frömling, H.L. Thaman, S. Berendts, R. Uecker, W.C. Carter, Y.-M. Chiang, Adv. Energy Mater. 7 (2017) 1701003.
[48] H.-K. Kang, S.-G. Woo, J.-H. Kim, S.-R. Lee, Y.-J. Kim, Electrochim. Acta 176 (2015) 172–178.
[49] R. Zhang, X. Chen, X. Shen, X.Q. Zhang, X.R. Chen, X.B. Cheng, C. Yan, C.Z. Zhao, Q. Zhang, Joule 2 (2018). http://dx.doi.org/10.1016/j.joule.2018.02.001.
[50] X. Shen, H. Liu, X.-B. Cheng, C. Yan, J.-Q. Huang, Energy Storage Mater. 12 (2018) 161–175.
[51] Z. Jiang, T. Liu, L. Yan, J. Liu, F. Dong, M. Ling, C. Liang, Z. Lin, Energy Storage Mater. 11 (2018) 267–273.
[52] X.-B. Cheng, T.-Z. Hou, R. Zhang, H.-J. Peng, C.-Z. Zhao, J.-Q. Huang, Q. Zhang, Adv. Mater. 28 (2016) 2888–2895.
[53] K. Yan, B. Sun, P. Munroe, G. Wang, Energy Storage Mater. 11 (2018) 127–133.
[54] W. Li, H. Yao, K. Yan, G. Zheng, Z. Liang, Y.-M. Chiang, Y. Cui, Nat. Commun. 6 (2015) 7436–7443.
[55] W. Liu, D. Lin, A. Pei, Y. Cui, J. Am. Chem. Soc. 138 (2016) 15443–15450.
[56] L. Wang, X. Zhu, Y. Guan, J. Zhang, F. Ai, W. Zhang, Y. Xiang, S. Vijayan, G. Li, Y. Huang, G. Cao, Y. Yang, H. Zhang, Energy Storage Mater. 11 (2018) 191–196.
[57] Y. Li, J. Jiao, J. Bi, X. Wang, Z. Wang, L. Chen, Nano Energy 32 (2017) 241–246.